A COMPARISON OF THE DYNAMIC LIFE CYCLES OF TROPOSPHERIC MEDIUM-SCALE WAVES AND STRATOSPHERIC PLANETARY WAVES

William J. Randel
National Center for Atmospheric Research
P. O. Box 3000
Boulder, CO 80303

ABSTRACT. This paper presents a comparison of the dynamic life cycles exhibited by a) baroclinically-forced medium-scale waves in the Southern Hemisphere (SH) troposphere, and b) tropospherically-forced, vertically-propagating planetary waves in the SH winter stratosphere. Cross correlation analyses of nine years of daily data reveal the characteristic EP flux signatures and wave-induced mean flow tendencies during wave growth, maturity and decay. Wave source and sink regions are shown, and strong midlatitude Rossby wave radiation towards low latitudes is observed in both instances. Tropospheric waves are shown to influence the zonal mean flow deep into the lower stratosphere (up to 30 mb). Wave-induced mean flow accelerations in the troposphere are to a large degree reversible between wave growth and decay, whereas the stratospheric waves exert a predominant one-way influence only (zonal flow deceleration). The midlatitude stratospheric waves are also shown to have a delayed, secondary influence in the subtropical upper stratosphere; this may be the statistical signature of planetary wave reflection (or overreflection) from a low latitude critical region.

1. Introduction

The life cycles of baroclinic waves in the troposphere have been studied extensively in the last decade, beginning with the pioneering modeling study by Simmons and Hoskins (1978). The dynamic life cycles of the waves in that idealized experiment were documented further in Edmon et al. (1980) and Hoskins (1983), based on zonal mean diagnostics. Observationally, Randel and Stanford (1985) documented a particularly clear baroclinic wave life cycle in the Southern Hemisphere (SH) troposphere during December 1979. The zonal wave number scale of these waves is observed to be $\sim$ k = 4-7, and they are termed 'medium-scale waves.' Medium scale waves often dominate circulation patterns in the SH troposphere (Salby, 1982; Hamilton, 1983).

Randel (1990) has studied the dynamical signatures of tropospheric wave life cycles statistically, by application of cross-correlation analyses to seven years of

A. O'Neill (ed.),
Dynamics, Transport and Photochemistry in the Middle Atmosphere of the Southern Hemisphere, 91–109.

operational data from the European Center for Medium Range Weather Forecasts (ECMWF). The advantage of using a statistical technique is that an immense amount of data may be studied concisely, and only coherent wave behavior which occurs repeatedly (and are thus in some sense 'real') are highlighted. Case studies of individual events are also valuable, and compliment statistical analyses. The statistical methodology is capable of revealing wave structure with high detail: for example, Randel (1990) documents Ferrel cell fluctuations associated with tropospheric baroclinic waves. Cross-correlation analyses are used here, and tropospheric results based on National Meteorological Center (NMC) data are presented.

Vertically propagating stratospheric planetary waves also exhibit clear life cycle characteristics, as illustrated in the cross-correlations and composited case study in Randel et al. (1987). The focus of this paper is to present a statistical analysis of stratospheric planetary wave life cycles, and make a comparison with the evolution observed of tropospheric waves. These comparisons reveal similarities in some aspects, such as the strong meridional propagation of Rossby wave activity from middle towards low latitudes during wave maturity and decay. There are also important differences; wave-induced mean flow changes in the stratosphere exhibit much less reversibility between wave growth and decay than that found in the troposphere. The correlations suggest some process which effectively damps stratospheric wave activity at low latitudes, with spatial and temporal signatures consistent with 'planetary wave breaking.' Additionally, the results show that a consistent feature of the stratospheric life cycles is a delayed reversal of the EP flux in the low latitude upper stratosphere. The nature of this remote, coherent behavior is not yet explained; one possibility is that it is the statistical signature of planetary wave reflection from a low latitude critical layer.

2. Data and Analyses

The data analyzed here are daily zonal mean wind, temperature and wave flux quantities derived from geopotential height grids over 1000-1 mb. Geopotential data over 1000-100 mb are NMC operational analyses, while data from 70-1 mb are Climate Analysis Center (CAC) operational products. Data are analyzed over 1979-1987. Horizontal winds are derived using linearized momentum equation balances. Additionally, daily analyses of zonal mean variables over 1000-100 mb from ECMWF are used; these are discussed in detail in Randel (1990).

Zonal mean diagnostics are based on the transformed Eulerian mean formalism. The zonal mean zonal momentum equation is:

$$\frac{\partial \bar{u}}{\partial t} = \hat{f}\bar{v}^* + D_F. \qquad (1)$$

Here $\hat{f} = 2\Omega\sin\phi - \frac{1}{a\cos\phi}\frac{\partial}{\partial\phi}(\cos\phi\bar{u})$, $\bar{v}^*$ is the meridional residual circulation, and

D_F is the quasi-geostrophic Eliassen-Palm flux divergence:

$$D_F = (\rho_s a \cos\phi)^{-1} \left[\frac{1}{a \cos\phi} \frac{\partial}{\partial \phi}(F_\phi) + \frac{\partial}{\partial z}(F_z) \right] \tag{2a}$$

$$(F_\phi, F_z) = \rho_s a \cos\phi \left[- \overline{u'v'}, \frac{R}{H} \hat{f} \frac{\overline{v'T'}}{N^2} \right]. \tag{2b}$$

Notation is standard, and may be referenced in Dunkerton et al. (1981).

The quasi-geostrophic wave activity equation is also used here, in the form

$$\frac{\partial}{\partial t} A + D_F = -\alpha A, \tag{3}$$

where the -αA term is a linear damping factor. A is defined as

$$A = \frac{1}{2} \overline{q'^2} / \overline{q}_y,$$

where q' is the quasi-geostrophic wave potential vorticity, and $\overline{q}_y$ the zonal mean potential vorticity gradient. Equation (3) is tested below by correlating $(\frac{\partial}{\partial t} + \alpha)$ A and D_F time series; for these calculations the time series are smoothed in both latitude and time with a 1-2-1 running filter.

Time lag cross-correlation analyses are used to find spatially coherent structure in the meridional plane and delineate the time evolution. The methodology used here is to choose one time series as a reference for midlatitude wave amplitude variations, and then use this time series as reference for correlating all other zonal mean variables throughout the meridional plane. The correlations here use wave kinetic energy at 300 mb, averaged over 40-50°S, as reference time series for the tropospheric waves, while the stratospheric calculations are referenced with respect to wave kinetic energy at 10 mb, averaged over 40-60°S. Results are not sensitive to the use of kinetic energy reference time series; identical results are obtained for geopotential variance or wave enstrophy. Correlation statistics are calculated from 90-day time series centered on each season; the tropospheric correlations are averaged over the four seasons and both hemispheres (because there is little variability with season or hemisphere), while stratospheric correlations shown here were calculated over August-October (the time of maximum stratospheric wave activity in the SH; qualitatively similar patterns are found for the NH winter). The SH stratospheric results do change somewhat with season; early and late winter correlations are contrasted in Randel (1988). 5% significance levels for the tropospheric correlations are near 0.06, and near 0.16 for the stratospheric patterns. Further details of these calculations may be found in Randel (1990).

3. Results

a. Tropospheric life cycles

Figure 1 shows EP flux correlation diagrams for the tropospheric wave life cycle. The vectors in Fig. 1 represent correlations (with respect to the 300 mb, 40-50° wave kinetic energy) at each position with the separate components of the EP flux vector; the horizontal component measures correlation with F_ϕ, likewise the vertical component with F_z. The contours denote correlations with the EP flux divergence D_F (Eq. 2a). Time lags in Fig. 1 are with respect to the wave energy time series, hence lags -2 and -1 day correspond to upper tropospheric, midlatitude wave growth, lag 0 to maturity, and lags +1 to +2 to wave decay. Important features revealed in Fig. 1 include:

1. Strong correlations with F_z (poleward heat flux) in the lower troposphere during wave growth and maturity; the heat flux correlations increase in the upper troposphere and lower stratosphere with time lag, consistent with vertical propagation of wave activity.
2. There is strong convergence of EP flux in midlatitudes (negative contours in Fig. 1) at lags -2 and -1 days (denoting local wave growth), and these correlations extend into the lower stratosphere (up to 30 mb) as the wave amplifies.
3. As the wave matures the upper tropospheric F_y (poleward momentum flux) correlations become strong, denoting propagation of wave activity to low latitudes. Coincident with this equatorward propagation is the loss of midlatitude wave activity (positive midlatitude D_F correlations at lags +1 to +2 days) and increase in low latitudes (negative correlations).

Note that these correlations represent deviations from the time mean patterns. As shown in Randel (1990), the actual daily variability in D_F is similar to that in Fig. 1 (with sign reversal in midlatitudes), whereas the time mean EP vectors are only modulated by these daily variations (the downward pointing arrows at lag +2 days in Fig. 1 indicate a reduction in poleward heat flux rather than absolute equatorward flux). The patterns in Fig. 1 are in good agreement with the baroclinic grow-barotropic decay life cycles modeled in Simmons and Hoskins (1978). Note the high degree of reversibility in the midlatitude correlations between wave growth and decay in Fig. 1.

Figure 2 presents correlation diagrams for zonal mean zonal wind acceleration $\frac{\partial \bar{u}}{\partial t}$ (top) and zonal mean temperature tendency $\frac{\partial \bar{T}}{\partial t}$ (bottom) for time lags -2, 0 and +2 days. During wave growth (lag -2 days) there is strong zonal wind deceleration in midlatitudes (negative correlations), flanked to both north and south by acceleration regions. The correlations are in phase vertically, extend deep into the lower stratosphere, and exhibit a meridional half wavelength of 15-20° latitude. These patterns are completely reversed at lag +2 days (wave decay), with midlatitude acceleration flanked meridionally by deceleration regions. There is good

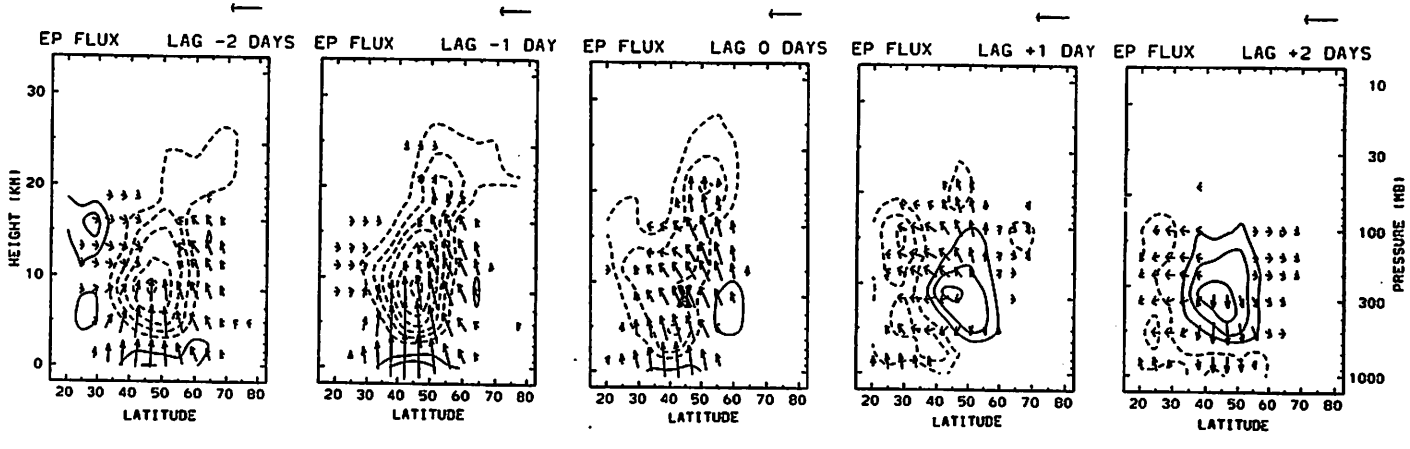

Figure 1. EP flux correlation diagrams for tropospheric wave life cycle, calculated as discussed in text. Vectors represent correlations with components of the EP flux vector, with the reference vector in the upper right hand corner representing a component correlation of 0.5. Contours represent correlations with D_F, with contour intervals of $\pm$ 0.05, 0.10, ...; 5% significance levels are near 0.06. The reference time series is wave kinetic energy at 300 mb, 40-50° (denoted by 'x' in lag 0 plot). Shown are correlations for time lags of -2 days (i.e., two days prior to wave kinetic energy maxima, left panel) to +2 days (right panel).

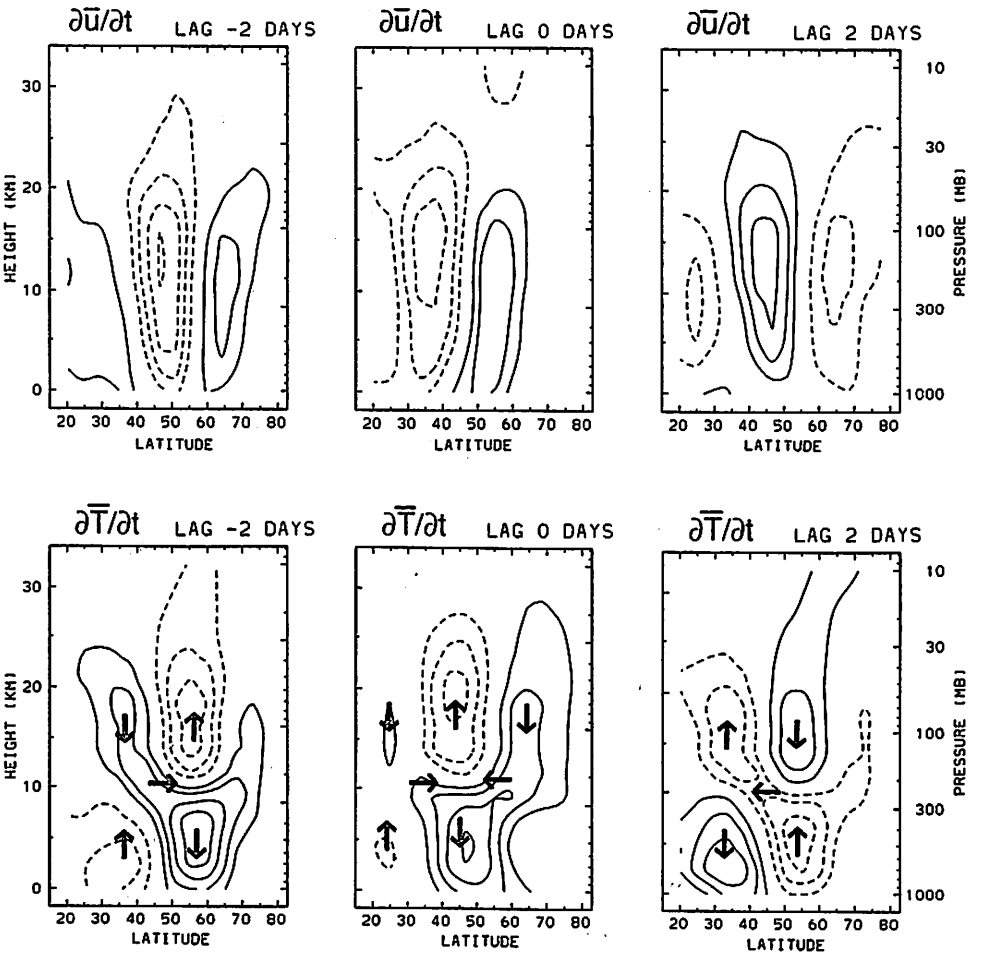

Figure 2. Meridional cross sections of correlations between wave kinetic energy at 300 mb, 40-50°, and zonal mean zonal wind acceleration ($\frac{\partial \bar{u}}{\partial t}$ - top panels) and zonal mean temperature tendency ($\frac{\partial \bar{T}}{\partial t}$ - lower panels). Shown are time lags of -2 days (left) to +2 days (right). Contours are ± 0.05, 0.10, ..., with positive values denoting accelerations and warmings, respectively. Also added in the lower panels are arrows denoting the residual circulation, as calculated explicitly in Randel (1990). Compare with the EP flux correlations in Fig. 1 (which are based on the same reference time series).

agreement between the central $\frac{\partial \bar{u}}{\partial t}$ correlations and the corresponding midlatitude D_F patterns in Fig. 1, although the D_F patterns are broader in latitude and shallower in the vertical. Randel (1990) shows observationally that the residual circulation acts to accentuate and narrow the meridional wavelike structure and deepen the vertical scale of the wave driving, such that there is near exact spatial agreement between ($\hat{f}\bar{v}^*$ + D_F) and ($\frac{\partial \bar{u}}{\partial t}$) correlations.

Zonal temperature tendency correlations in Fig. 2 during wave growth (lag -2 days) show high latitude warming and low latitude cooling over 0-10 km, with oppositely-signed patterns over 10-20 km, such that overall there is a quadrupole pattern in the meridional plane. This spatial structure is in good agreement with that anticipated due to localized wave driving, e.g., Dunkerton et al. (1981) and Garcia (1987). Note that these temperature tendencies are in thermal wind balance with the observed $\frac{\partial \bar{u}}{\partial t}$ patterns. Included in Fig. 2 are vectors representing residual circulation correlations; these are calculated explicitly in Randel (1990), and found to be in good agreement with the temperature tendencies. During wave decay (lag +2 days) the $\frac{\partial \hat{T}}{\partial t}$ and residual circulation patterns are opposite those during wave growth, again showing a high degree of reversibility between wave growth and decay.

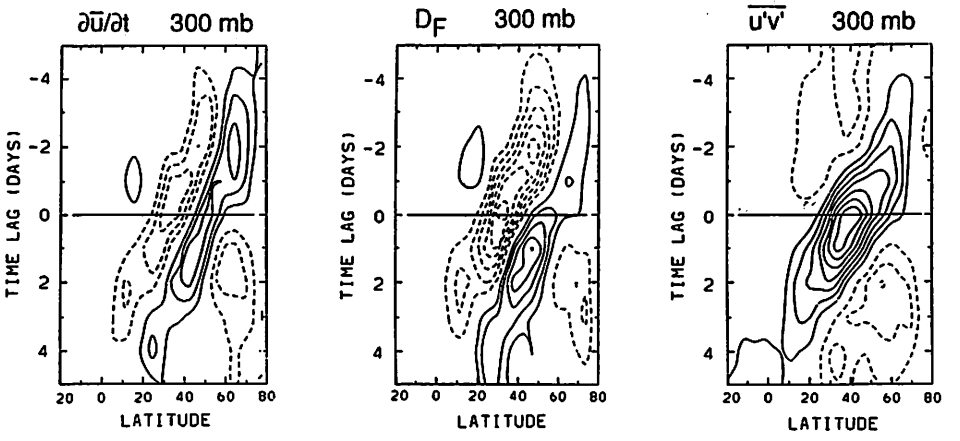

Figure 3. Latitude-time lag sections of correlations (as in Figs. 1-2) for tropospheric wave life cycles. These are calculated using ECMWF data for the SH only. a) shows $\frac{\partial \bar{u}}{\partial t}$ correlations at 300 mb, and b) shows D_F correlations at 300 mb, using reference kinetic energy time series at 40-50°S; note the good spatial and temporal agreement between (a) and (b), and propagation of anomalies to low latitudes. c) Shows $\overline{u'v'}$ correlations at 300 mb; positive contours denote poleward $\overline{u'v'}$.

Figure 3a shows a latitude-time diagram of the $\frac{\partial \bar{u}}{\partial t}$ correlations at 300 mb, illustrating the time development of wave-induced zonal wind accelerations. In this figure ECMWF data were used in order to extend the wave flux calculations equatorward of 20° (the NMC/CAC geopotential-derived fluxes are poor in low latitudes). Clear equatorward propagation of the $\frac{\partial \bar{u}}{\partial t}$ anomalies is seen in Fig. 3a, with a speed near 7° latitude per day ($\sim$ 10 m/s). Figure 3b shows a similar diagram for D_F correlations, also illustrating strong equatorward propagation (and agreement with the $\frac{\partial \bar{u}}{\partial t}$ patterns). Note these correlations extend deep into the tropics. This tropical influence of midlatitude waves is further demonstrated in Fig. 3c, where a latitude-time section of momentum flux correlations are shown; there is a suggestion in this figure of coherent momentum flux anomalies which extend beyond the equator. The strong equatorward propagation seen in these statistics lends credence to the idealized barotropic decay modeled by Held and Phillips (1987).

b. Stratospheric life cycles

Figure 4 shows EP flux correlation diagrams for stratospheric planetary wave life cycles. The reference time series is wave kinetic energy at 10 mb, averaged over 40-60°. Only zonal waves 1-2 are used to calculate the zonal mean wave flux quantities; inclusion of higher zonal wave numbers does not change the stratospheric correlations, but reduces the upper tropospheric patterns (due to inclusion of incoherent medium-scale wave fluctuations). Features of planetary wave evolution revealed in Fig. 4 include:

1. Strong correlation with F_z over 45-70° above $\sim$ 300 mb during wave growth (lags -4 and -2 days), showing vertical propagation in this region. There is convergence of EP flux in the lower-middle stratosphere at this time, consistent with local wave growth. The F_z correlations are discontinuous below 300 mb, and there is little evidence of coherent vertical propagation below this level. Consistent with this discontinuity in F_z is a region of positive D_F correlation in the high latitude upper troposphere at lags -2 and 0 days, suggesting a local source of planetary wave activity in this region. This upper tropospheric source region was discussed in Randel et al. (1987), and may be attributable to nonlinear forcing from medium scale waves (*in situ* instability is not possible here because $\bar{q}_y > 0$). There are also weak correlations in the lower troposphere which suggest that *in situ* (baroclinic) planetary wave generation may be of assistance in triggering these stratospheric wave events.
2. The strongest vector correlations move upwards and somewhat equatorwards in the stratosphere as the wave matures, and correlations with F_y are dominant at lag +2 days (showing the dominance of barotropic processes). Coincident with these F_y correlations is a strong high latitude region of positive D_F correlation, with low latitude negative contours (a north-south dipole pattern); note the similarity to the tropospheric patterns at lag +1 day (Fig. 1).

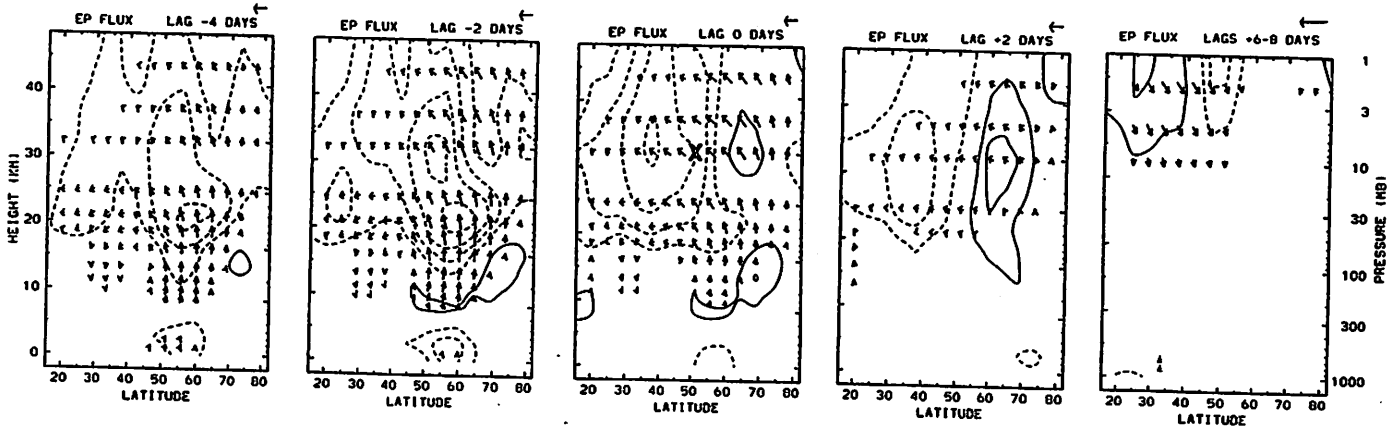

Figure 4. EP flux correlation diagrams (as in Fig. 1) for stratospheric planetary wave life cycles (note reference position at 10 mb in lag 0 plot). Time lags of -4, -2, 0, +2 and the average of +6 to +8 days. Arrows in the last panel are doubled for clarity. Contours of ± 0.1, 0.2, ..., with 5% significance levels near 0.16. Note the vertical axis is 1000-1 mb, versus 1000-10 mb in Fig. 1.

3. Approximately one week following the maximum kinetic energy at 10 mb in midlatitudes (lags +6 to +8 days in Fig. 4), the low latitude upper stratosphere exhibits positive D_F correlations equatorward of negative patterns (a north-south dipole pattern of opposite polarity to that seen in midlatitudes at lag +2 days). There are poleward and downward pointing EP flux correlations in this region at this time; this is a reversal of the EP flux patterns seen in midlatitudes throughout lags -4 to +2 days.

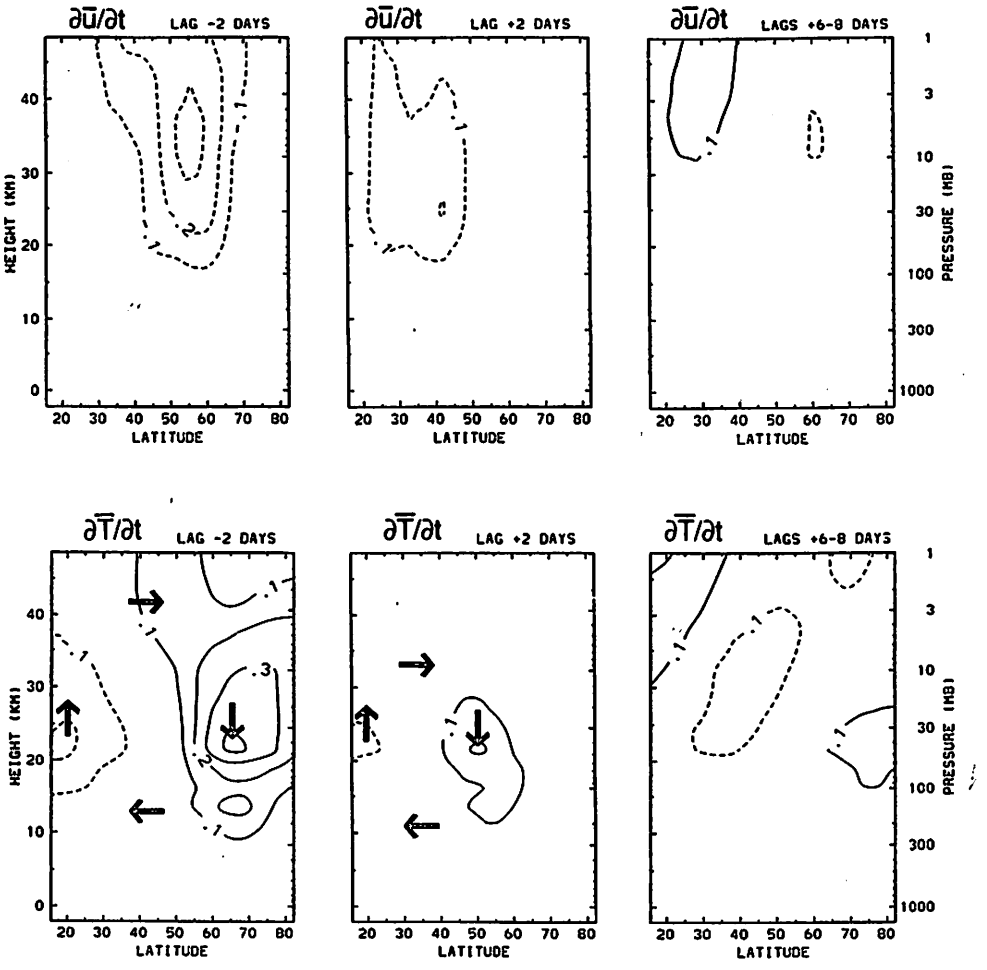

Figure 5. $\frac{\partial \bar{u}}{\partial t}$ (top) and $\frac{\partial \bar{T}}{\partial t}$ (bottom) correlation sections (as in Fig. 2) for stratospheric life cycles, for time lags -2, +2 and the average of +6 to +8 days. Contours of ± 0.1, 0.2, ...

Figure 5 shows meridional sections of $\frac{\partial \bar{u}}{\partial T}$ and $\frac{\partial \bar{T}}{\partial t}$ correlations for the stratospheric life cycles, at lags -2, +2 and +6 to +8 days. There is strong middle to high latitude $\bar{u}$ deceleration over 100-1 mb (and above) at lag -2 days, weakening and moving to lower latitudes at lag +2 days. The lag -2 day $\frac{\partial \bar{T}}{\partial t}$ patterns show strong polar warming and low latitude cooling centered near 100-10 mb, and there are presumably patterns of opposite polarity above 1 mb (e.g., Garcia, 1987) not seen in these data. The $\bar{u}$ deceleration regions approximately follow the equatorward movement of the negative D_F correlations seen in Fig. 4. This is shown more clearly in the 10 mb latitude-time lag sections for $\frac{\partial \bar{u}}{\partial t}$ and D_F correlations in Figs. 6a-b. At 1 mb (Figs. 6c-d), there is less evidence of meridional movement of the correlation patterns. Randel (1988) shows that these $\frac{\partial \bar{u}}{\partial t}$ correlations change seasonally in such a way that early winter wind changes are at lower latitude than those in late winter-spring, i.e., the waves are more confined to high latitudes in spring.

The lag +6 to +8 day $\frac{\partial \bar{u}}{\partial t}$ correlations in Fig. 5 show subtropical acceleration in upper levels in the same location as the positive D_F contours at lags +6 to +8 days in Fig. 4. These similar spatial patterns are also seen in the 1 mb sections in Figs. 6c-d, where the time lag of approximately 1 week with respect to midlatitude events is emphasized. NH correlations (not shown) exhibit qualitatively similar patterns, with a somewhat longer time delay (of order $\sim$ 10 days).

The delayed low latitude patterns seen in both wave and mean flow statistics is an intriguing result which deserves further comment. Figure 7 shows time series of selected variables for one year (1981) used for the correlation statistics. The middle stratospheric reference kinetic energy time series is shown, along with 100 mb heat flux; these series demonstrate the episodic nature of planetary wave events. Also shown are time series for low latitude, upper stratospheric $\overline{u'v'}$, D_F and $\frac{\partial \bar{u}}{\partial t}$. Arrows in Fig. 7 denote episodes of poleward F_ϕ (positive $\overline{u'v'}$) and positive D_F (and $\frac{\partial \bar{u}}{\partial t}$) which lag by approximately one week the midlatitude kinetic energy maxima. Inspection of individual time series from other years shows some events with positive D_F and poleward F_ϕ in these regions (as in Fig. 7), but more often there is only a modulation (not a reversal) of the climatological values here. A similar low latitude EP flux vector and D_F pattern is shown in Hitchman et al. (1987), their Fig. 6, with a similar time lag relationship with midlatitude Rossby wave events. They suggest such patterns may result from inertial instability in the tropical mesosphere, forced as a result of meridionally propagating midlatitude Rossby waves. However, the patterns shown here are substantially removed from the equator, and thus not likely due to that mechanism. The location and timing of these reversed F_ϕ patterns, in conjunction with weak zonal winds in low latitudes, is suggestive of a reflection of planetary wave activity near a critical line (where wave phase velocity equals zonal wind speed). These patterns may be the statistical signature of such planetary wave reflection. In the case where additionally $\bar{q}_y < 0$, the waves may 'overreflect' and extract energy from the mean flow (Dunkerton, 1987). Figure 8 shows $\bar{u}$ and $\bar{q}_y$ during 18-24 August, 1981 (c.f. Fig. 7), and indeed there is a region of $\bar{q}_y < 0$ in the upper stratosphere on the equatorward flank of the jet.

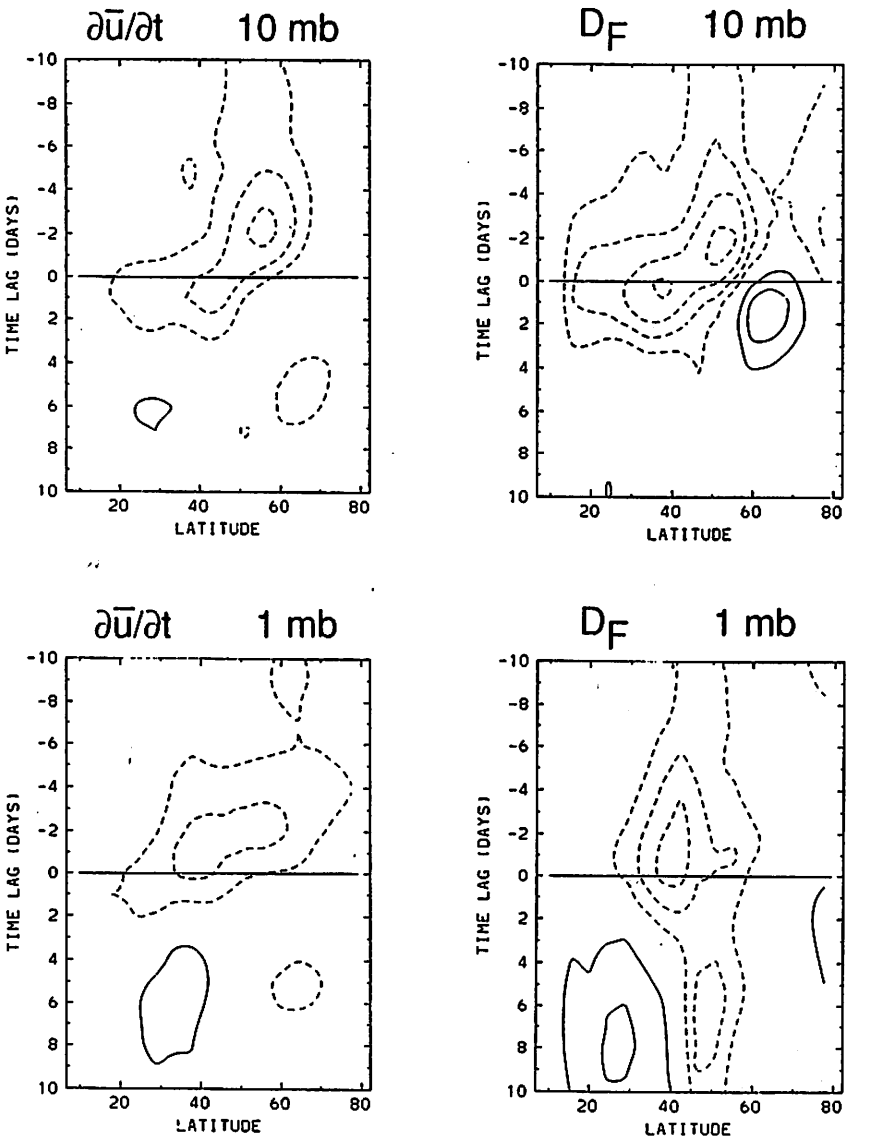

Figure 6. Latitude-time lag correlation sections for stratospheric life cycles. Shown are $\frac{\partial \bar{u}}{\partial t}$ (left) and D_F (right) patterns at 10 mb (top) and 1 mb (bottom). Contours of $\pm$ 0.1, 0.2, ... Note the overall spatial and temporal agreement in the $\frac{\partial \bar{u}}{\partial t}$ and D_F patterns at both levels.

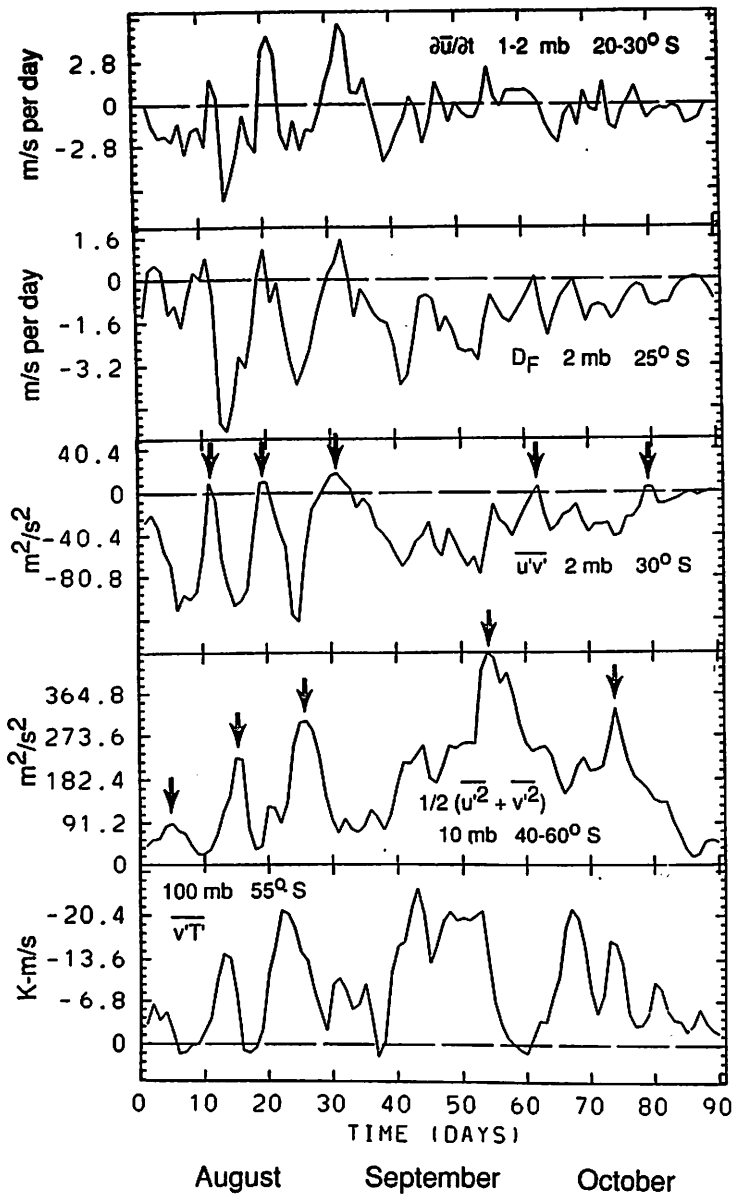

Figure 7. Time series of planetary wave variations during August-October, 1981. The variables and locations are listed; note the kinetic energy time series (second from bottom) which is used as reference for all the correlation sections. Arrows denote midlatitude wave events and the time-lagged, positive $\overline{u'v'}$ in the subtropical upper stratosphere.

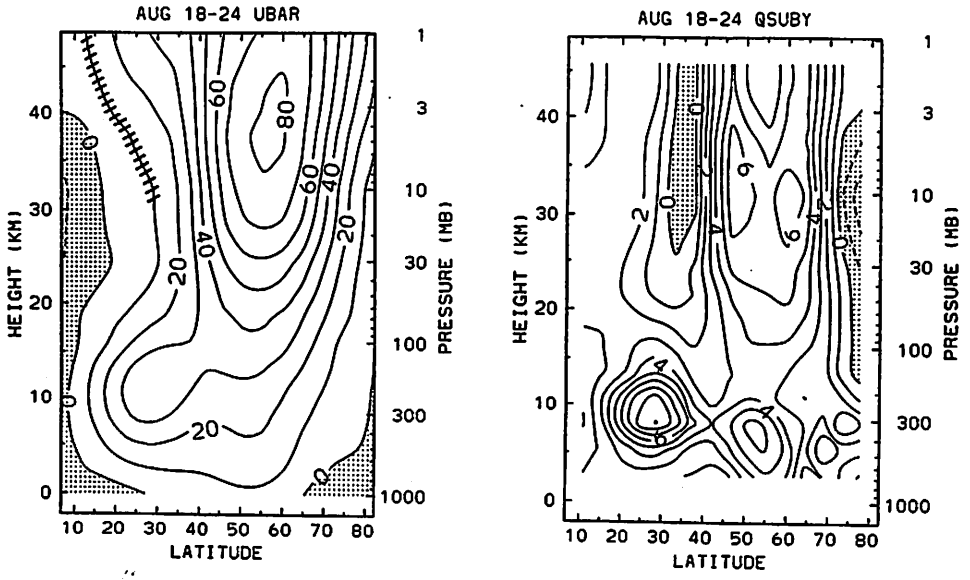

Figure 8. Meridional cross sections of zonal mean zonal wind $\bar{u}$ (m/s) and quasi-geostrophic potential vorticity gradient $\bar{q}_y$ (10^{-11} $m^{-1}s^{-1}$) averaged over 18-24 August, 1981. The hatched region in the $\bar{u}$ plot denotes the approximate location of the critical line for eastward propagating waves in SH winter ($c \sim 10$ m/s). Note the negative $\bar{q}_y$ region over 30-40°S. Wave statistics during this period are shown in Fig. 7.

A further aspect of planetary wave life cycles is revealed by study of the wave activity equation, including a linear damping term (Eq. 3). Figure 9 shows a meridional cross-section of the contemporaneous $(\frac{\partial}{\partial t} + \alpha)$ A vs. D_F correlation with no damping ($\alpha = 0$), along with a similar section using a damping time scale of 2 days ($\alpha = (2 \text{ days})^{-1}$). Both diagrams show correlations of order 0.2 - 0.4 throughout the troposphere, and there is little qualitative change with the addition of the damping term. In contrast, the stratospheric correlations increase dramatically in low latitudes and decrease somewhat in high latitudes when the damping term is included, suggesting that dissipation is important in low (but not high) latitudes.

Figure 10 shows plots of the 20°-70° average $(\frac{\partial}{\partial t} + \alpha)$ A vs. D_F correlation as a function of α at 400, 50 and 2 mb; a similar plot from NH data is also included. These plots show a dramatic increase in 2 mb correlation as more damping is added, up to 1-2 day time scales; this is the reason 2 days was chosen for Fig. 9 (note that patterns similar to Fig. 9 are found for NH data). Correlations at 50

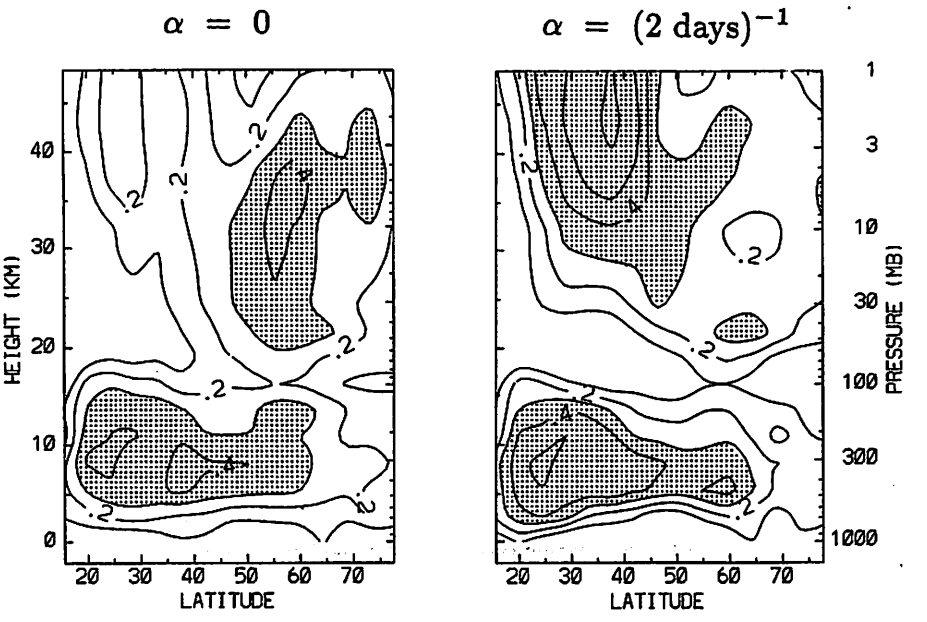

Figure 9. Meridional cross sections of the contemporaneous correlation between $(\frac{\partial}{\partial t} + \alpha)$ A and D_F (Eqn. 3) for $\alpha = 0$ (no damping) and $\alpha = (2 \text{ days})^{-1}$ (2 day damping time scale). Contours of 0.1, 0.2, ..., and correlations above 0.3 are stippled. Note the strong increase in correlation in the low latitude upper stratosphere when the damping term is included.

and 400 mb show near constant values as the damping is increased up to 1-2 day time scales, deteriorating substantially for stronger values. Overall, the correlations in Figs. 9-10 suggest some effective wave damping in the low latitude upper stratosphere, with an effective time scale of order 2 days. This location and time scale is in good agreement with stratospheric surf zone – planetary wave breaking ideas (McIntyre and Palmer, 1984), because wave breaking should occur preferentially in low latitudes (Baldwin and Holton, 1988), with a time scale consistent with advective processes ($\sim$ a few days). Note that radiative damping times in this region are of order $\sim$ 10-20 days (Kiehl and Solomon, 1986, their Fig. 5), and hence radiative processes are probably not the source of this damping.

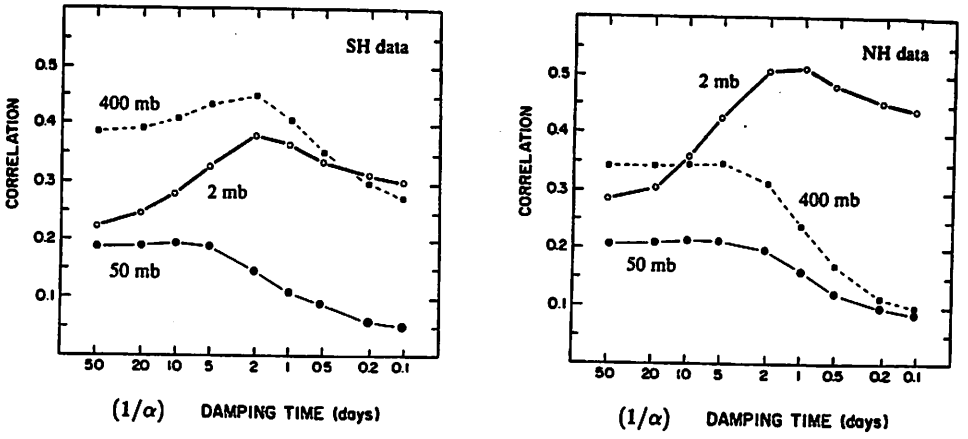

Figure 10. $(\frac{\partial}{\partial t} + \alpha)$ A vs. D_F correlation coefficients, averaged over 20-70°, at 2, 50 and 400 mb, plotted as function of linear damping time scale $(1/\alpha)$. Note the strong increase in correlation at 2 mb as damping time approaches 1-2 days. Data for SH correlations (left) and NH correlations (right).

4. Comparison of Life Cycles: Similarities and Differences

The above correlation analyses have yielded statistical pictures of the wave and mean flow patterns which repeatedly occur in association with wave amplification/decay in the troposphere and stratosphere. Similarities are pointed out to underscore common dynamical processes, while differences are highlighted to focus on distinct physical situations.

a. Similarities

Both life cycles exhibit strong correlations with F_z (poleward eddy heat flux) below the region of and prior to wave growth. For tropospheric waves, this is lower tropospheric heat flux coincident with *in situ* baroclinic wave growth, while for stratospheric waves this corresponds to propagation from the upper troposphere (as noted above, *in situ* baroclinic generation of the planetary waves in the upper troposphere is prohibited because $\bar{q}_y > 0$).

An unmistakable similarity in these life cycles is the propagation of midlatitude wave activity towards low latitudes as the waves mature and decay. This is seen clearly in the strong equatorward F_y and north-south dipole patterns in D_F for the mature waves in Figs. 1 and 4. The preferential refraction of Rossby waves towards low latitudes results from the spherical geometry (see the discussion in Palmer, 1982).

b. Differences

Perhaps the most striking difference between the life cycles is the degree of reversibility seen in the tropospheric cycle (the lag +2 days patterns in Figs. 1-2 are all nearly opposite those at lag -2 days; note especially the mean flow tendencies), while there is little reversibility seen in the stratosphere. The midlatitude mean flow decelerates as the tropospheric waves grow, then re-accelerates as the waves radiate to low latitudes. Conversely, the stratosphere waves primarily decelerate the zonal flow during wave growth and maturity (Figs. 5-6); there is little evidence of rapid zonal acceleration as the waves decay. This is consistent with planetary waves which propagate into the stratosphere and dissipate (either mechanically or radiatively), as opposed to tropospheric waves which propagate strongly out of midlatitudes before they decay. Wave activity correlations also point to the importance of some damping process in the stratosphere, and show that it occurs preferentially in the low latitude upper stratosphere with a time scale of order 2 days. This location and time scale is consistent with a 'stratospheric surf zone – planetary wave breaking' hypothesis (McIntyre and Palmer, 1984).

The stratospheric correlations also show intriguing low latitude, upper stratospheric reversed EP flux and D_F patterns, which follow by approximately one week midlatitude, middle stratospheric wave amplitude maxima. The reality of these correlations are supported by similar spatial and temporal signatures in D_F and $\frac{\partial \bar{u}}{\partial t}$ (Figs. 6c-d), and in their similar appearance in NH data (not shown). The poleward F_ϕ and positive D_F correlations here are usually associated with a modulation ('turning off') of the climatological patterns in this region, although occasionally actual reversals occur. The location and timing of the reversed F_ϕ patterns suggest that they may be the statistical signature of planetary wave reflection from the low latitude critical region. The positive $\frac{\partial \bar{u}}{\partial t}$ accelerations at this time could result from radiative re-acceleration following wave events, or from direct wave-induced effects ('overreflection,' e.g., Dunkerton, 1987). Although details of these patterns await explanation, their occurrence in the present correlation analyses demonstrate that they are repeatable aspects of the planetary wave life cycle.

Acknowledgments

The author thanks Byron Boville for discussions and comments, and Tim Dunkerton and Michael McIntyre for comments on the text. Marilena Stone expertly prepared the manuscript. This work has been partly supported under NASA Grant W-16215. NCAR is sponsored by the National Science Foundation.

References

Baldwin, M. P. and J. R. Holton, 1988: Climatology of the stratospheric polar vortex and planetary wave breaking. *J. Atmos. Sci., 45*, 1123-1142.

Dunkerton, T. J., 1987: Resonant excitation of hemispheric barotropic instability in the winter mesosphere. *J. Atmos. Sci., 44*, 2237-2251.

Dunkerton, T. J., C.-P.F. Hsu and M. E. McIntyre, 1981: Some Eulerian and Lagrangian diagnostics for a model stratospheric warming. *J. Atmos. Sci., 38*, 819-843.

Edmon, H. J., Jr., B. J. Hoskins and M. E. McIntyre, 1980: Eliassen-Palm cross sections for the troposphere. *J. Atmos. Sci., 37*, 2600-2616; also corrigendum, *J. Atmos. Sci., 38*, 1115 (1981).

Garcia, R. R., 1987: On the mean meridional circulation of the middle atmosphere. *J. Atmos. Sci., 44*, 3599-3609.

Hamilton, K., 1983: Aspects of wave behavior in the mid and upper troposphere of the southern hemisphere. *Atmos. Ocean, 21*, 40-54.

Held, I. M. and P. J. Phillips, 1987: Linear and nonlinear barotropic decay on the sphere. *J. Atmos. Sci., 44*, 200-207.

Hitchman, M. H., C. B. Leovy, J. C. Gille and P. L. Bailey, 1987: Quasi-stationary, zonally asymmetric circulations in the equatorial middle atmosphere. *J. Atmos. Sci., 44*, 2219-2236.

Hoskins, B. J., 1983: Modelling of the transient eddies and their feedback on the mean flow. Large-Scale Dynamical Processes in the Atmosphere, B. J. Hoskins and R. P. Pearce, Eds. Academic Press, 397 pp.

Kiehl, J. T. and S. Solomon, 1986: On the radiative balance of the stratosphere. *J. Atmos. Sci., 43*, 1525-1534.

McIntyre, M. E. and T. N. Palmer, 1984: The 'surf zone' in the stratosphere. *J. Atmos. Terr. Phys., 46*, 825-849.

Palmer, T. N., 1982: Properties of the Eliassen-Palm flux for planetary scale motions. *J. Atmos. Sci., 39*, 992-997.

Randel, W. J., 1988: The seasonal evolution of planetary waves in the southern hemisphere stratosphere and troposhere. *Quart. J. Roy. Meteor. Soc., 114*, 1385-1409.

Randel, W. J., 1990: Coherent wave-zonal mean flow interactions in the troposphere. *J. Atmos. Sci., 47*, 439-456.

Randel, W. J. and J. L. Stanford, 1985: The observed life cycle of a baroclinic instability. *J. Atmos. Sci., 42*, 1364-1373.

Randel, W. J., D. E. Stevens and J. L. Stanford, 1987: A study of planetary waves in the southern winter troposphere and stratosphere. Part II: Life cycles. *J. Atmos. Sci., 44*, 936-949.

Salby, M. L., 1982: A ubiquitous wave number-5 anomaly in the southern hemisphere during FGGE. *Mon. Wea. Rev., 110*, 1712-1720.

Simmons, A. J. and B. J. Hoskins, 1978: The life cycles of some nonlinear baroclinic waves. *J. Atmos. Sci., 35*, 414-432.